

Modeling and Simulation of Soft Robots driven by Artificial Muscles: an Example using Twisted-and-Coiled Actuators

Jiefeng Sun and Jianguo Zhao

Abstract—Soft robots have been intensively investigated for manipulation and locomotion in recent years. However, the current state of soft robotics has significant design and development work but lags in modeling and control due to the difficulty in modeling them. In this paper, we present a physics-based analytical framework to model soft robots driven by Twisted-and-Coiled Actuators (TCAs), an artificial muscle that can be arranged in arbitrary shapes in the soft body of a soft robot to achieve programmable motions. The framework can model 1) the complicated routes of multiple TCAs in a soft body and 2) the coupling effect between the soft body and the TCAs during their actuation process. When not actuated, a TCA in the soft body is an antagonistic elastic element that restrains the magnitude of the motion and increases the stiffness of the robot. By stacking several modules together, we simulate the sequential motion of a soft robotics arm with three-dimensional bending, twisting, and grasping motion. The presented modeling and simulation approach will facilitate the design, optimization, and control of soft robots driven by TCAs or other types of artificial muscles.

I. INTRODUCTION

Soft robots are a new type of robot with deformable bodies and muscle-like actuation, which are fundamentally different from traditional robots with rigid links and motor-based actuators. Owing to their elasticity, soft robots outperform rigid ones in safety, maneuverability, and adaptability [1]. With their advantages, many soft robots have been developed for manipulation and locomotion in recent years. Soft robots have found their uses in a wide number of fields such as medical applications [2] and biologically-inspired locomotion [3]. In these applications, soft robots have been demonstrated to be resilient and highly adaptable, benefiting applications like locomotion, gripping, and improved human interactions.

To actuate soft robots, we can use artificial muscles. Among all the artificial muscles, a low-cost one has recently emerged: a twisted-and-coiled actuator (TCA), which has high energy density, and is relatively easy to fabricate [4]–[6]. Its tendon-like slender shape and compliance of bending allow us to arrange it in a soft body in an arbitrary shape to create complicated and programmable motions. Due to the aforementioned merits, many TCA-driven soft robots has been developed such as: bending beams [7], soft crawlers [8], soft bistable gripper [9], shape morphing skin [10], robotics arm [11], and robotic jellyfish [12].

* This work is partially supported by National Science Foundation under grants IIS-1755766

Jiefeng Sun and Jianguo Zhao are with Department of Mechanical Engineering, Colorado State University, Fort Collins, CO 80523, USA. J.Sun@colostate.edu, Jianguo.Zhao@colostate.edu

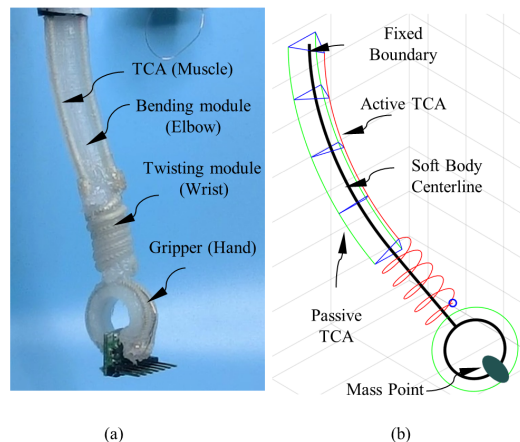


Fig. 1. (a) The TCA-driven soft robotics arm picks up a PCB board; (b) The simulated soft robotics arm.

Despite increasing applications, the current state of artificial muscle-driven soft robots has significant design and development work, but lags behind in modeling and simulation due to the complex behavior of the soft bodies, artificial muscles, and their coupling. Those soft bodies endow soft robots with infinite degrees of freedom that are significantly more complex than traditional rigid robots. Modeling such robots is complicated due to the need of continuum models of the soft body [13]. Also, it is challenging to model the coupling between the soft body and the artificial muscle. The problem can be further complicated by the irregular or arbitrary routes of these artificial muscles in the soft body.

To address the challenges, we have used Cosserat rod model that can accurately model continuum robots [14], [15] to model TCA-driven soft robots [16]. But the previously proposed method only considered the simplest case where only a straight TCA is actuated to drive a soft manipulator. However, the real cases could be more complicated with one example of a soft robotic arm shown in Fig. 1(a) [11]. The robotics arm has three serially connected modules: a 3D bending module, a twisting module, and a gripper. Our previous work cannot handle such a robotic arm correctly [17]. First, when three TCAs are arranged in parallel inside a soft body, the actuated TCA will need to overcome the antagonistic stretching force of the other two unactuated/passive TCAs, resulting in a much less actuation magnitude. Second, the twisting module has a TCA arranged in a helical route and this is usually difficult to model using conventional simplified methods such as the piece-wise constant curvature

method. Third, several modules can be combined together to realized more complicated motions, introducing the coupling problem between neighboring modules.

To address these issues, we aim to establish a more general modeling framework using Cosserat rod theory. The model will consider the actuation and coupling between multiple TCAs, allow us to simulate complex motion generated from the irregular routes of the TCAs, and realize the combination of motions. Our method is different from some recent research on simulation of shape memory alloy (SMA) driven robot [18] and musculoskeletal systems [19]. Both of them generate actuation by shifting reference states of a rod or directly applying general force and moment on a part of the rod; therefore usually there is no implicit coupling between a robot and the artificial muscle. Unlike these works, our method considers the coupling between an artificial muscle and the soft body, and the implicit artificial muscles' forces needed to be solved during the process. Since these phenomena exist for soft robots driven by other artificial muscles (e.g., dielectric elastomers, liquid crystal elastomers), we expect our method can also be used for modeling and simulating those robots.

The rest of this paper is organized as follows. In Section II, We introduce the modeling framework for soft robots driven by TCAs. In Section III, we present the numerical method to solve a single module and serially connected modules. In Section IV, the simulation results for a single 3D bending module and the soft robotics arm are presented. In Section IV, we conclude the paper and discuss future research directions.

II. ANALYTICAL MODELING

A soft body actuated by TCAs is modeled as a single Cosserat rod. In this section, we provide a brief overview of the system of ODEs from a Cosserat rod, and introduce how to incorporate an external load such as gravity, actuation force from the artificial muscle, i.e., TCAs, and the coupling between the artificial muscle and the soft body.

A. Kinematics

In Cosserat theory, bodies are modeled as a collection of infinitesimal rigid bodies (IRBs) rather than point particles, and thus each IRB has both position and orientation rather than just position. For a given rod, we define the centerline, $s \in [0, L]$, as the curve passing through the centroids of all the cross sections where L is the length of the rod in its reference configuration. At every point s along the centerline, we establish a body frame for the cross section. The z axis of the frame is tangent to s and the x and y axes are assumed to be aligned with the principal axes of the cross sections. Each body frame has a rotation and a translation relative to the global (fixed) frame. We describe the position and orientation of all the IRBs along the centerline using a homogeneous transformation matrix $g(s) \in SE(3)$.

$$g(s) = \begin{bmatrix} R(s) & p(s) \\ 0 & 1 \end{bmatrix} \quad (1)$$

where $R(s) \in SO(3)$ is a rotation matrix and $p(s) \in \mathbb{R}^3$ is the position vector.

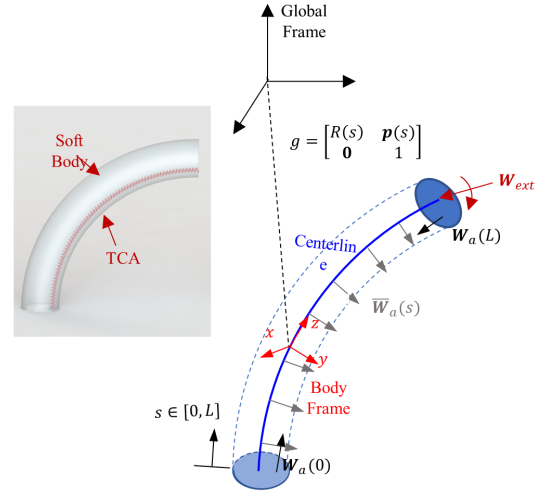


Fig. 2. A soft body driven by a single artificial muscle and its corresponding diagram of the kinematics using the Cosserat rod theory. It shows the centerline $s \in [0, L]$ as the blue solid curve, the configuration g , and the body frame (in red) attached to a cross section.

With $g(s)$, the system of ODEs for the kinematics and statics can be written as [15]:

$$g' = g\hat{\xi} \quad (2)$$

$$\mathbf{W}_i = K\Delta\xi \quad (3)$$

$$\bar{\mathbf{W}}_e - ad_{\xi}^T \mathbf{W}_i + \mathbf{W}'_i = 0 \quad (4)$$

where $'$ is the derivative with respect to s , and $\xi = [u^T, v^T]^T \in \mathbb{R}^6$ is the spatial twist (strain) representing the relative configuration change between adjacent cross sections along the centerline, with $u, v \in \mathbb{R}^3$ the angular and linear strain component, respectively. The 'hat' operator $\hat{\cdot}$ is a mapping from \mathbb{R}^3 to $\mathfrak{so}(3)$ or \mathbb{R}^6 to $\mathfrak{se}(3)$, e.g., $\hat{\xi} = \begin{bmatrix} \hat{u} & v \\ 0 & 0 \end{bmatrix}$,

$\bar{\mathbf{W}}_e = [\bar{l}^T, \bar{f}^T]^T$ is the distributed external wrench with $\bar{l}, \bar{f} \in \mathbb{R}^3$ as the moment, force per unit arclength applied to the centerline in the body frame, $ad_{\xi} = \begin{bmatrix} \hat{u} & 0 \\ v & \hat{u} \end{bmatrix}$ is adjoint

representation of the spatial twist ξ . $\mathbf{W}_i = [m^T, n^T]^T$ is the internal wrench in the body frame with $m, n \in \mathbb{R}^3$ as the internal moment and force in the body frame. $K_{bt} = \mathbf{diag}[EI_x, EI_y, GJ]$ is the diagonal stiffness matrix for bending and torsion, and $K_{se} = \mathbf{diag}[GA_t, GA_t, EA_t]$ is the diagonal stiffness matrix for shear and extension. E and G are the Young's modulus and shear modulus, respectively. A_t is the cross section area of the rod, I_x, I_y are the second moment of area with respect to x and y axis, and $J = I_x + I_y$ is the polar moment of inertia of the rod's cross section about its centroid.

We decompose (2) into the angular and linear component to facilitate our numerical simulation using non-unit quaternion, and rewrite the system of ODEs using R, p , and ξ as

state variables

$$R' = R\hat{u} \quad (5)$$

$$\mathbf{p}' = R\mathbf{v} \quad (6)$$

$$\boldsymbol{\xi}' = K^{-1}(\text{ad}_{\boldsymbol{\xi}}^T K \Delta \boldsymbol{\xi} - \bar{\mathbf{W}}_e) + \boldsymbol{\xi}'^* \quad (7)$$

External distributed wrench comes from the artificial muscle and gravity

$$\bar{\mathbf{W}}_e = \bar{\mathbf{W}}_{grav} + \bar{\mathbf{W}}_a \quad (8)$$

where

$$\bar{\mathbf{W}}_{grav} = \rho A \begin{bmatrix} \mathbf{0}_{3 \times 1} \\ R^T \mathbf{g}_r \end{bmatrix}, \quad (9)$$

is the distributed gravitational force in the global frame, and $\mathbf{g}_r = [0, 0, 9.81]^T$ is the gravitational vector. $\bar{\mathbf{W}}_a$ is the distributed wrench due to the artificial muscle TCA's tension force.

Note that the TCA-driven soft robots is different from tendon-driven robots since a TCA has two anchoring points on the body and the wrench exerted on a robot is considered as an internal wrench that does not influence the segment where the TCAs is not embedded as shown in Fig. 2. Therefore, the initial and distal boundary condition need to be adjusted as

$$\mathbf{W}_i(0) = \mathbf{W}_{i,0} - \mathbf{W}_a \quad (10)$$

$$\mathbf{W}_i(L) = \mathbf{W}_a + \mathbf{W}_{ext} \quad (11)$$

where $\mathbf{W}_{i,0}$ is the initial internal wrench if the TCA is connected to the ground, \mathbf{W}_a is the sum of point wrench exerted by TCAs, and \mathbf{W}_{ext} is the sum of explicit external wrench applied to the distal end.

B. TCA Force Mapped to the Rod

A TCA is embedded into a soft body by running through a channel in the soft body and the channel is created during the soft body's fabrication process [11]. The friction force between the TCA and the soft body is negligible. We assume that the TCA is able to freely slide in the channels and the TCA only has axial loads (no bending stiffness). This derivation is general for any wire artificial muscle.

In the following, we derive the wrench exerted by i^{th} TCA to the centerline of the rod in the global frame

$$\mathbf{W}_{a,i}^g = F_a \begin{bmatrix} \hat{\mathbf{p}}_a \mathbf{t}_a \\ \mathbf{t}_a \end{bmatrix} \quad (12)$$

where the superscript g indicates that the wrench is represented in the global frame. F_a is the tension force in the TCA, $\mathbf{p}_a = R\mathbf{r}_a + \mathbf{p}$ is the position of the TCA in the global frame, and $\mathbf{r}_a = [x_a, y_a, 0]^T$ is the position vector of the TCA in the body frame. $\mathbf{t}_a = \frac{\mathbf{p}'_a}{\|\mathbf{p}'_a\|}$ is the unit tangent vector to the TCA, where

$$\mathbf{p}'_a = \frac{\partial(R\mathbf{r}_a + \mathbf{p})}{\partial s} = R(\mathbf{v} - \hat{\mathbf{r}}_a \mathbf{u} + \mathbf{r}'_a) \quad (13)$$

To get the distributed wrench, we take the derivative of (12) with respect to s .

$$\bar{\mathbf{W}}_{a,i}^g = \frac{\partial \mathbf{W}_{a,i}^g}{\partial s} = F_a \begin{bmatrix} \hat{\mathbf{p}}'_a \mathbf{t}_a + \hat{\mathbf{p}}_a \mathbf{t}'_a \\ \mathbf{t}'_a \end{bmatrix} + F'_a \begin{bmatrix} \hat{\mathbf{p}}_a \mathbf{t}_a \\ \mathbf{t}_a \end{bmatrix} \quad (14)$$

Note that $\hat{\mathbf{p}}'_a \mathbf{t}_a = 0$

$$\bar{\mathbf{W}}_{a,i}^g = F \begin{bmatrix} \hat{\mathbf{p}}_a \mathbf{t}_a \\ \mathbf{t}_a \end{bmatrix} + F' \begin{bmatrix} \hat{\mathbf{p}}_a \mathbf{t}_a \\ \mathbf{t}_a \end{bmatrix} \quad (15)$$

Since the balance equation (7) is established in the body frame. We need to map the distributed wrench and point wrench back to the body frame using the adjoint transformation and note that $F' = 0$, $\hat{\mathbf{p}}_a - \hat{\mathbf{p}} = (R\mathbf{r}_a)' = R\hat{\mathbf{r}}_a R^T$ leading to:

$$\bar{\mathbf{W}}_{a,i} = \text{Ad}_g^T \bar{\mathbf{W}}_{a,i}^g = F \begin{bmatrix} \hat{\mathbf{r}}_a R^T \mathbf{t}_a \\ R^T \mathbf{t}_a \end{bmatrix} \quad (16)$$

where $\text{Ad}_g^T = \begin{bmatrix} R^T & -R^T \hat{\mathbf{p}} \\ 0 & R^T \end{bmatrix}$ is the transpose of adjoint transformation.

We also need the following to calculate the explicit form of the cable wrench, and represent it with strains [14]

$$\mathbf{t}'_a = -\frac{(\hat{\mathbf{p}}'_a)^2}{\|\mathbf{p}'_a\|^3} \mathbf{p}''_a$$

$$\mathbf{p}''_a = R(\hat{\mathbf{u}}(\mathbf{v} - \hat{\mathbf{r}}_a \mathbf{u} + \mathbf{r}'_a) + \mathbf{v}' - \hat{\mathbf{r}}_a \mathbf{u}' - \hat{\mathbf{r}}'_a \mathbf{u} + \mathbf{r}''_a)$$

Therefore $R^T \mathbf{t}'_a$ term in Eq. (16) that appears both in moment and the force term is

$$\begin{aligned} R^T \mathbf{t}'_a &= -R^T \frac{(\hat{\mathbf{p}}'_a)^2}{\|\mathbf{p}'_a\|^3} \mathbf{p}''_a \\ &= P\mathbf{v}' - P\hat{\mathbf{r}}_a \mathbf{u}' + b - P(\hat{\mathbf{r}}'_a \mathbf{u} - \mathbf{r}''_a) \end{aligned} \quad (17)$$

where $b = P(\hat{\mathbf{u}}(\mathbf{v} - \hat{\mathbf{r}}_a \mathbf{u} + \mathbf{r}'_a))$, $P = -R^T \frac{(\hat{\mathbf{p}}'_a)^2}{\|\mathbf{p}'_a\|^3} R$

We can split $\bar{\mathbf{W}}_a$ and \mathbf{W}_a into components that do and do not depend on $\boldsymbol{\xi}'$

$$\bar{\mathbf{W}}_{a,i} = \bar{A}_i \boldsymbol{\xi}' + \bar{B}_i \quad (18)$$

where

$$\bar{A}_i = F_a \begin{bmatrix} -\hat{\mathbf{r}}_a P \hat{\mathbf{r}}_a & \hat{\mathbf{r}}_a P \\ -P \hat{\mathbf{r}}_a & P \end{bmatrix}, \quad \bar{B}_i = F_a \begin{bmatrix} \hat{\mathbf{r}}_a (b - P(\hat{\mathbf{r}}'_a \mathbf{u} - \mathbf{r}''_a)) \\ b - P(\hat{\mathbf{r}}'_a \mathbf{u} - \mathbf{r}''_a) \end{bmatrix}$$

Both $\bar{A}_i \in \mathbb{R}^{6 \times 6}$ and $\bar{B}_i \in \mathbb{R}^6$ are independent of $\boldsymbol{\xi}'$, but dependent on $\boldsymbol{\xi}$. It is simple to use $\boldsymbol{\xi}$ instead of \mathbf{W}_i as the state variables because of the dependence of $\bar{\mathbf{W}}_a$ on $\boldsymbol{\xi}$ and $\boldsymbol{\xi}'$.

The ends of the TCAs are always fixed to the soft body, typically the ends. In this case, a TCA will exert a of point wrench due to the tension. This can be written in the body frame as:

$$\mathbf{W}_{a,i} = \text{Ad}_g^T \mathbf{W}_{a,i}^g = F_a \begin{bmatrix} \hat{\mathbf{r}}_a R^T \mathbf{t}_a \\ R^T \mathbf{t}_a \end{bmatrix} \quad (19)$$

If there are n TCAs arranged in the soft body, the total distributed will be

$$\bar{\mathbf{W}}_a = \bar{A} \boldsymbol{\xi}' + \bar{B} \quad (20)$$

$$\mathbf{W}_a = \sum_{i=1}^n \mathbf{W}_{a,i} \quad (21)$$

where $\bar{A} = \sum_{i=1}^n \bar{A}_i$ and $\bar{B} = \sum_{i=1}^n \bar{B}_i$

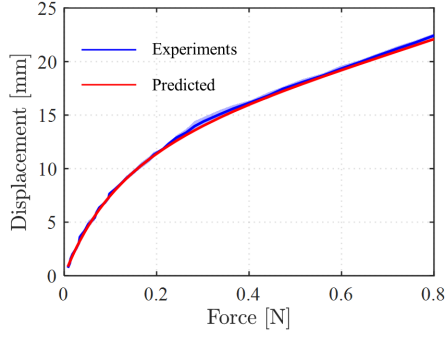


Fig. 3. The experimental and predicted results of the passive displacement of a TCA with respect to external force.

C. TCA Model and Coupling to the Rod

The TCA's displacement and tension force are both coupled to the rod's deformation. The displacement of a TCA can be calculated from the positions of the TCA coupled to the soft body

$$\delta_a = \int_0^L \|\mathbf{p}'_a\| ds - \int_0^L \|(p_a^*)'\| ds \quad (22)$$

where δ_a is the displacement of the TCA, and this is the difference of the TCA's arc length between the current configuration and the original configuration.

TCAs can be modeled using castigliano's Second Theorem (CST) [20]

$$\delta_a = A_{cst} \Delta \bar{\theta}^h - \frac{1}{K_{cst}} F_a \quad (23)$$

where $\Delta \bar{\theta}^h$ is the unit untwisting of a twisted fiber used to fabricate TCAs with respect to temperature. A polynomial can be used to approximate $\Delta \bar{\theta}^h = -0.0161T^2 + 0.3338T - 7.7311$ based on our previous work, and

$$\frac{1}{K_{cst}} = l_t \left(\frac{r^2 \cos^2 \alpha}{G_t J_t} \right), A_{cst} = l_t r \cos \alpha$$

r is the TCA's diameter, l_t is the twisted fiber's length, A_t is the cross section area of the twisted fiber, and α is the pitch angle of the TCA. Note that based on the small deformation assumption, all the variables are close to their values of the reference states, for example, $\alpha \approx \alpha^*$. We also ignored the bending, shear, and extension strain of the TCA for simplicity.

However, when a TCA is not actuated, it will act as a nonlinear mechanical spring. Its share modulus G_t gradually increases with respect to the TCA's stretching deformation, resulting in increasing stiffness for a passive TCA. We conduct experiments to measure the stretching force of a TCA with its deformation and fit G_t using a 2nd order polynomial with respect to the TCA's external force, $G_t = 37.58Fa^2 + 111.33Fa + 0.85$ MPa. With such a fitting, the predicted passive displacement is pretty close to our experimental results as shown in Fig. 3.

Combining (22) and (23), we can have an compatibility equation for the TCA

$$\int_0^L \|\mathbf{p}'_a\| ds - l^* - (A_{cst} \Delta \bar{\theta}^h - \frac{1}{K_{cst}} F_a) = 0. \quad (24)$$

Plugging (20) in (8) and (7), and rearrange to make ξ' explicit, we have

$$\xi' = (K + \bar{A})^{-1} (ad_{\xi}^T K \Delta \xi - \bar{B} - \bar{W}_{grav} + K \xi^*). \quad (25)$$

Rearranging (10) and (11), we can obtain

$$\xi(0) = \xi_0 - K^{-1} \mathbf{W}_a \quad (26)$$

$$\xi(L) = K^{-1} (\mathbf{W}_a + \mathbf{W}_{ext}) + \xi^* \quad (27)$$

where ξ_0 is the initial strain if the TCA is connected to the ground.

A single module driven by a TCA can be fully defined by the system of ODEs (5), (6) and (25) with compatibility equation (24) and boundary condition (26) and (27).

III. NUMERICAL IMPLEMENTATIONS

A. Quaternions as Rotation

Spatial derivative of rotations (R') is integrated using non-unit quaternions to avoid truncation error and ensure $R \in \text{SO}(3)$ [21]. This method allows any high-order integration scheme or general-purpose ODE solver to efficiently integrate rotations over a long spatial range while eliminating singularities and maintaining the structure of $\text{SO}(3)$. The basic idea is to replace integration of R' with the integration of \mathbf{h}' .

A quaternion $\mathbf{h} = h_0 + h_1i + h_2j + h_3k$, where i, j , and k are called quaternionic units. \mathbf{h} can be written in a vector form in \mathbb{R}^4 : $\mathbf{h} = [h_0, h_1, h_2, h_3]^T$. Then we can have the derivative of \mathbf{h} with respect to s as [21]

$$\mathbf{h}' = \frac{1}{2} \Omega \mathbf{h} \quad (28)$$

where

$$\Omega = \begin{bmatrix} 0 & -u_x & -u_y & -u_z \\ u_x & 0 & u_z & -u_y \\ u_y & -u_z & 0 & u_x \\ u_z & u_y & -u_x & 0 \end{bmatrix}$$

u_x, u_y and u_z are elements of \mathbf{u} . We can convert R between \mathbf{h} using existing algorithms *quat2rotm* and *rotm2quat* in Matlab.

B. Shooting method Solving Connected Rods

TCA actuation force F_a is an implicit variable that is required both for the boundary condition and for the ODEs. A shooting method can be used to solve the boundary value problem with the unknown implicit force. The method starts from guessing the initial strain $\xi(0)$ and the actuation forces F_a for the TCAs using the trust-region-dogleg method. Then the ODEs are integrated from $s = 0$ to $s = L$ using a standard library code (e.g., *ode45* in Matlab), during which the distributed wrench and point wrenches will need to be calculated. Finally, the boundary conditions and the compatibility equation are checked. If the a residual error

ϵ as in (29) is within specified tolerance, the algorithm stops and returns the results, otherwise new guess values will be generated and the process repeats until the boundary conditions and the compatibility equations are satisfied.

$$\epsilon = \left[\int_0^L \|p'_a\| ds - l^* - (A_{cst} \Delta \bar{\theta}^h - \frac{1}{K_{cst}} F_a) \right] \quad (29)$$

If two or more rods are serially connected, a piece-wise integration needs to be implemented to solve them together as shown in Algorithm 1. For this case, we only guess the very first rod's initial condition to make sure that the very last rod's distal boundary condition and the compatibility equation for each TCA are satisfied.

Algorithm 1: Solving serially connected modules

Input: Temperature vectors of the TCAs
Initiate parameters;
Setup Initial boundary conditions g_0 ;
for $T = T_0 \rightarrow T_{max}$ **do**
 while $\epsilon > Tol$ **do**
 Guess ξ_0 for the first rod;
 Adjust the initial boundary Eq. (26);
 Integrate the first module Eqs. (5), (6) and (25);
 Adjust the distal boundary condition to include point forces Eq. (27);
 Use the distal boundary of first module as the initial boundary condition of the second module;
 Adjust the initial boundary Eq. (26);
 Integrate the second module Eqs. (5), (6) and (25);
 Return the error of the compatibility equations of all TCAs, and the distal boundary condition of the second module Eq. (29).
 end
 Visualization;
end

IV. RESULTS

We use the 3D bending module and the soft robotics arm as examples to illustrate the simulation of a single module and serially connected modules. We use Young's modulus $E = 0.125$ MPa and $G = E/3$ for the soft body made of Ecoflex-30 (Smooth On Inc.). The 3D bending module and twisting module are simplified as a rod with circular cross section that has a diameter of 4.5 mm. The gripper's cross section is a rectangular shape of 3×6 mm.

A. Simulation of a Single 3D Bending Module

The 3D bending module has three TCAs located 4 mm from the center at the angle of 0, 120, and 240° as shown in the inset of Fig. 4. The length of the soft body and the TCA is 45 mm. We simulate the case that TCA 2 and 3 are actuated, and TCA 1 serves as a passive TCA that

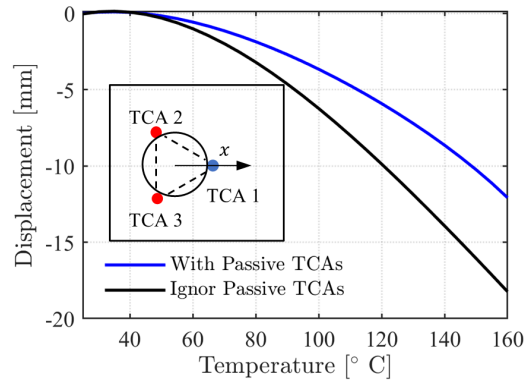


Fig. 4. The comparison between the cases with and without considering the antagonistic forces from the passive TCAs. The inset shows the cross section of the 3D bending module and the actuated TCAs.

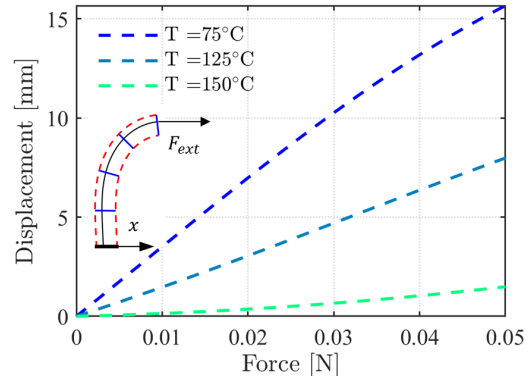


Fig. 5. The displacement of the 3D bending module with respect to a horizontal force demonstrating the variable stiffness function of the module. The inset shows the direction diagram of the applied force on the module.

generate antagonistic forces. Figure 4 shows that the bending magnitude without considering the passive TCAs is more than 40% larger than the case considering the passive TCAs' antagonistic forces. The error could be even larger when a stiffer material is used or the module has different geometry parameters. The results suggest that antagonistic force cannot be ignored if multiple TCAs are embedded in the module.

With this model, we can also simulate the variable stiffness effect of the 3D bending module when all three TCAs are equally actuated at the same time. Figure 5 shows the displacement of the module with respect to a force along x direction. When the temperatures of the 3 TCAs are increased from 75 to 125 °C, the same amount of force can cause much less displacement.

B. Simulation of the Soft Robotics Arm

The soft robotics arm shown in Fig.1 is realized by serially stacking a twisting module and a gripper (pre-curved 2D bending module) on the top of the 3D bending module. The TCA in the twisting module is wrapped on a soft cylinder (16 mm) in a helical shape located 3.5 mm from the center. There are total 5 rounds of TCAs and the two ends of the TCA is fixed on the cylinder. The gripper has a circular body shape and is normally closed, which means When the TCA

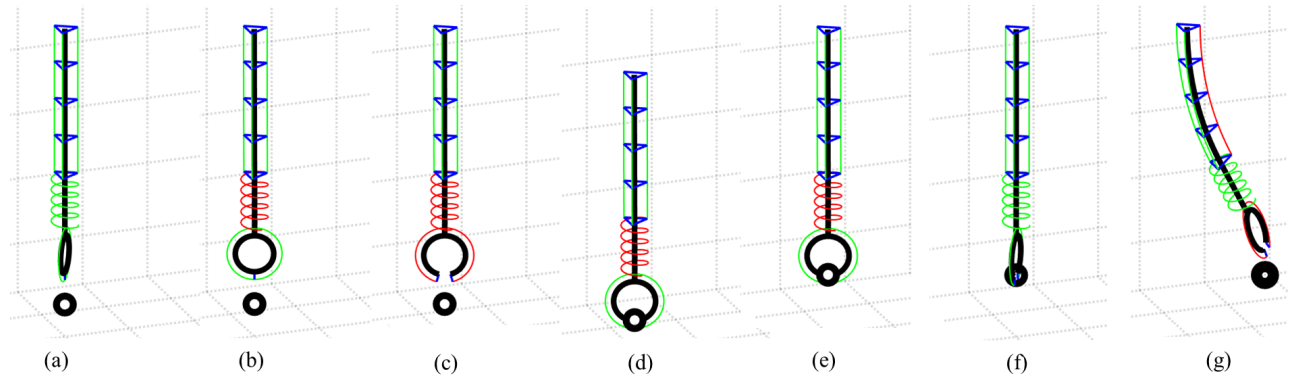


Fig. 6. The simulation of a pick-and-place process of the soft robotics arm. The red and green lines represent the active and passive TCAs, respectively. The centerlines of the soft bodies are represented by the thicker black lines. The blue lines illustrate the cross sections of the 3D bending module. (a) The initial straight configuration. The object is 10 mm under the gripper. (b) The twisting module rotates the gripper to align it with the object. (c) The gripper opens. (d) The arm is lowered and the gripper closes to pinch the object. (e) The arm lifts the object. (f) The twisting module is deactivated to rotate the gripper to its original orientation. (g) The bending module bends to x direction, and the gripper opens again to release the object to a different location.

contracts, the gripper can open it self. Therefore it holds objects when the TCA is not actuated and the TCA is located 2.5 mm from the center of the gripper's cross section.

Due to the small size of the gripper, only the 3D bending module and the twisting module are treated as serially connected modules that are solved together. The weight of the gripper and the object grasped by the gripper are considered as an external load that can be mapped to the tip of the twisting module.

Figure 6 shows the simulation of the robotics arm that conducts a pick-and-place task. First, the robotics arm is at its initial straight configuration. Then the twisting module rotates the gripper to allow it to align with the object. The gripper opens to pinch the object. The 3D bending module bends to the desired direction, and then the object is released by the gripper.

V. CONCLUSIONS

In this paper, we use TCA-driven soft robots as an example to present a general analytical model using Cosserat rod theory for soft robots driven by an artificial muscle. The model solves the coupling implicit force of the artificial muscles with deformation of the soft body, and considers the antagonistic force of passive artificial muscles. The simulation scheme for serially connected modules is also presented for simulating more general and complicated cases.

For future work, we will 1) conduct experiments to study the accuracy of the model; 2) include other examples that a different artificial muscle (e.g., shape memory alloy wires, pneumatic actuators) are used to verify the generality of the framework; 3) improve the computational efficiency of the framework; 4) expand the statics model to the dynamics.

REFERENCES

- [1] D. Rus and M. T. Tolley, "Design, fabrication and control of soft robots," *Nature*, vol. 521, no. 7553, pp. 467–475, 2015.
- [2] J. Burgner-Kahrs, D. C. Rucker, and H. Choset, "Continuum robots for medical applications: A survey," *IEEE Transactions on Robotics*, vol. 31, no. 6, pp. 1261–1280, Dec 2015.
- [3] Y. Tang, Y. Chi, J. Sun, T.-H. Huang, O. H. Maghsoudi, A. Spence, J. Zhao, H. Su, and J. Yin, "Leveraging elastic instabilities for amplified performance: Spine-inspired high-speed and high-force soft robots," *Science advances*, vol. 6, no. 19, p. eaaz6912, 2020.
- [4] C. S. Haines, M. D. Lima, N. Li, G. M. Spinks, J. Foroughi, J. D. Madden, S. H. Kim, S. Fang, M. J. de Andrade, F. Göktepe *et al.*, "Artificial muscles from fishing line and sewing thread," *science*, vol. 343, no. 6173, pp. 868–872, 2014.
- [5] G. M. Spinks, N. D. Martino, S. Naficy, D. J. Shepherd, and J. Foroughi, "Dual high-stroke and high-work capacity artificial muscles inspired by dna supercoiling," *Science Robotics*, vol. 6, no. 53, 2021.
- [6] D. R. Higuera-Ruiz, M. W. Shafer, and H. P. Feigenbaum, "Cavatappi artificial muscles from drawing, twisting, and coiling polymer tubes," *Science Robotics*, vol. 6, no. 53, 2021.
- [7] J. Zhang, "Modeling of a bending supercoiled polymer (scp) artificial muscle," *IEEE Robotics and Automation Letters*, vol. 5, no. 3, pp. 3822–3829, 2020.
- [8] Y. Yang, Y. A. Tse, Y. Zhang, Z. Kan, and M. Y. Wang, "A low-cost inchworm-inspired soft robot driven by supercoiled polymer artificial muscle," in *2019 2nd IEEE International Conference on Soft Robotics (RoboSoft)*. IEEE, 2019, pp. 161–166.
- [9] J. Sun, B. Tighe, and J. Zhao, "Tuning the energy landscape of soft robots for fast and strong motion," in *2020 IEEE/RSJ International Conference on Intelligent Robots and Systems (IROS)*. IEEE, 2020, pp. 10 082–10 088.
- [10] C. Lamuta, H. He, K. Zhang, M. Rogalski, N. Sottos, and S. Tawfick, "Digital texture voxels for stretchable morphing skin applications," *Advanced Materials Technologies*, vol. 4, no. 8, p. 1900260, 2019.
- [11] J. Sun, B. Tighe, Y. Liu, and J. Zhao, "Twisted-and-coiled actuators with free strokes enable soft robots with programmable motions," *Soft robotics*, vol. 8, no. 2, pp. 213–225, 2021.
- [12] A. Hamidi, Y. Almubarak, Y. M. Rupawat, J. Warren, and Y. Tadesse, "Poly-saora robotic jellyfish: swimming underwater by twisted and coiled polymer actuators," *Smart Materials and Structures*, vol. 29, no. 4, p. 045039, 2020.
- [13] O. M. O'Reilly, *Modeling nonlinear problems in the mechanics of strings and rods*. Springer, 2017.
- [14] D. C. Rucker and R. J. Webster III, "Statics and dynamics of continuum robots with general tendon routing and external loading," *IEEE Transactions on Robotics*, vol. 27, no. 6, pp. 1033–1044, 2011.
- [15] F. Renda, M. Giorelli, M. Calisti, M. Cianchetti, and C. Laschi, "Dynamic model of a multibending soft robot arm driven by cables," *IEEE Transactions on Robotics*, vol. 30, no. 5, pp. 1109–1122, 2014.
- [16] B. Pawlowski, J. Sun, J. Xu, Y. Liu, and J. Zhao, "Modeling of soft robots actuated by twisted-and-coiled actuators," *IEEE/ASME Transactions on Mechatronics*, vol. 24, no. 1, pp. 5–15, 2018.
- [17] B. Pawlowski, J. Sun, and J. Zhao, "Dynamic modeling of soft manipulators actuated by twisted-and-coiled actuators," in *2018 IEEE Conference on Decision and Control (CDC)*. IEEE, 2018, pp. 409–414.

- [18] W. Huang, X. Huang, C. Majidi, and M. K. Jawed, "Dynamic simulation of articulated soft robots," *Nature communications*, vol. 11, no. 1, pp. 1–9, 2020.
- [19] X. Zhang, F. K. Chan, T. Parthasarathy, and M. Gazzola, "Modeling and simulation of complex dynamic musculoskeletal architectures," *Nature communications*, vol. 10, no. 1, pp. 1–12, 2019.
- [20] J. Sun and J. Zhao, "Physics-based modeling of twisted-and-coiled actuators using cosserat rod theory," *IEEE Transactions on Robotics*, 2021.
- [21] C. Rucker, "Integrating rotations using nonunit quaternions," *IEEE Robotics and Automation Letters*, vol. 3, no. 4, pp. 2979–2986, 2018.